



VCU

Virginia Commonwealth University
VCU Scholars Compass

Theses and Dissertations


Graduate School

2022

Effects of Additive Manufacturing Techniques on the Magnetocaloric Properties and Chemical Stability of LaFexCoySi_{13-x-y} Alloys

Binyam Wodajo
Virginia Commonwealth University

Follow this and additional works at: <https://scholarscompass.vcu.edu/etd>

 Part of the [Manufacturing Commons](#), [Other Materials Science and Engineering Commons](#), and the [Polymer and Organic Materials Commons](#)

© The Author

Downloaded from

<https://scholarscompass.vcu.edu/etd/7053>

This Thesis is brought to you for free and open access by the Graduate School at VCU Scholars Compass. It has been accepted for inclusion in Theses and Dissertations by an authorized administrator of VCU Scholars Compass. For more information, please contact libcompass@vcu.edu.

Effects of Additive Manufacturing Techniques on the Magnetocaloric Properties and Chemical Stability of $\text{LaFe}_x\text{Co}_y\text{Si}_{13-x-y}$ Alloys

A thesis submitted in partial fulfillment of the requirements for the degree of Master of Science in Mechanical Engineering at Virginia Commonwealth University

By

Binyam Wodajo

Master of Science in Mechanical and Nuclear Engineering, Virginia Commonwealth University, 2022

Advisor: Radhika Barua Ph.D.

Department of Mechanical and Nuclear Engineering

Virginia Commonwealth University

Richmond, Virginia

May 8, 2022

Acknowledgments

I would like to take this opportunity to thank God first and foremost. I would then like to thank my parents for their undying efforts to help me succeed in my studies. I would also like to thank my advisor, Dr Barua, for continuously working with me on this research and guiding me every step of the way. Special thanks goes to Dr Hadimani and Dr Zhao and their respective labs for providing technical assistance as well as equipment that was used in the study. Finally, I want to thank everyone in our VIP team that has helped me with my research.

Contents

| | | |
|--------|--|----|
| 1 | Introduction..... | 9 |
| 1.1. | Energy Consumption | 9 |
| 1.2. | Current Refrigeration Technology | 9 |
| 1.3. | Alternative methods for refrigeration..... | 11 |
| 2 | Magnetic Cooling | 14 |
| 2.1. | Overview of Magnetocaloric Technology | 14 |
| 2.2. | Challenges Toward System Integration | 16 |
| 2.3. | Problem Statement | 17 |
| 3 | Experimental Methods..... | 21 |
| 3.1. | Powder Sample Preparation | 21 |
| 3.2. | 3D Printed Sample Preparation..... | 22 |
| 3.3. | Characterization Methods | 23 |
| 3.3.1. | Scanning Electron Microscopy | 23 |
| 3.3.2. | X-Ray Diffraction | 23 |
| 3.3.3. | Magnetofunctional Response | 24 |
| 3.4. | Chemical Stability and Corrosion..... | 26 |
| 4 | Results..... | 29 |
| 4.1. | Microstructural properties and Composition of Precursor Powders and 3D Printed Samples ... | 29 |
| 4.2. | Magneto functional properties of precursor powders and 3D printed samples..... | 30 |
| 4.2.1. | Temperature and Field Dependent Magnetization | 30 |
| 4.2.2. | Magnetic Entropy Change | 31 |
| 4.3. | Chemical Stability of Precursor Powders | 31 |
| 4.3.1. | Microstructure and Phase Compositions of Powders after Immersion in Water | 31 |
| 4.3.2. | Magnetofunctional Response of Immersed Precursor Powders..... | 32 |
| 4.4. | Chemical Stability of 3D Printed Samples..... | 34 |
| 5 | Conclusion | 36 |
| 5.1. | Summary..... | 36 |
| 5.2. | Future Work..... | 37 |
| 6 | References..... | 39 |

List of Figures

| | |
|---|----|
| Figure 1: Global share of total energy supply by source in 1973 (left) and 2019 (right) [1] ----- | 9 |
| Figure 2: Vapor compression Cycle [2]----- | 10 |
| Figure 3: Magnetic Regenerator System Design working in a) Reciprocating Magnetic Field and b) Rotary Magnetic Field [18]. ----- | 16 |
| Figure 4: Different conformations and shapes of magnetocaloric regenerators (left) and Statistical distribution of heat exchange fluids and architectures of materials used to fabricate magnetocaloric regenerator prototypes (right) [18] ----- | 17 |
| Figure 5: Milling apparatus [28] ----- | 21 |
| Figure 6: Arc melting process [45] ----- | 21 |
| Figure 7. Visual representation of (a) Temperature-dependent magnetization curve; (b) Field-dependent magnetization curve [42]----- | 25 |
| Figure 8: Visual representation of a magnetic entropy change curve [34] ----- | 26 |
| Figure 9: Corrosion test rig for powder samples ----- | 27 |
| Figure 10. Immersion setup for 3D printed scaffold [43] ----- | 27 |
| Figure 11: XRD peaks for precursor powders and 3D printed scaffolds of LaFeSiCo samples ----- | 29 |
| Figure 12: Temperature (0.1T) and field dependent (300K) magnetization curves for the precursor powder and polymer blended 3D sample----- | 30 |
| Figure 13: Entropy change of LaFeCoSi powders and 3D printed pieces----- | 31 |
| Figure 14: Bragg peaks of LaFeCoSi precursor powders immersed in deionized water for up to 31 days | 32 |
| Figure 15: M-T, M-H and ΔS_{mag} curves of water immersed samples ----- | 33 |

List of Tables

| | |
|--|----|
| Table 1: Comparison of attributes of state-of-the-art magnetocaloric alloys [18]----- | 19 |
| Table 2: Magnetic properties of the precursor powders and the 3D printed samples----- | 30 |
| Table 3: T_c , M_s , and ΔS comparisons of immersed and non-immersed precursor powders ----- | 34 |
| Table 4: Various additive manufacturing methods used for producing magnetocaloric regenerators ----- | 37 |

Abstract

Title of Thesis: Effects of Additive Manufacturing Techniques on the Magnetocaloric Properties and Chemical Stability of $\text{LaFe}_x\text{Co}_y\text{Si}_{13-x-y}$ Alloys

By Binyam Wodajo

Bachelor of Science in Mechanical Engineering

A thesis submitted in partial fulfillment of the requirements for the degree of Master of Science in Engineering at Virginia Commonwealth University.

Virginia Commonwealth University, 2022

Thesis Advisor: Radhika Barua, Ph.D.

Professor, Department of Mechanical and Nuclear Engineering

Abstract

Keywords: Extrusion-based, Magnetic Entropy, Chemical Stability

Additive manufacturing (AM) is an emerging process to fabricate net shape, intricate, engineering components with minimal material waste; however, traditionally it has been largely applied to structural materials. AM of functional materials, such as magnetic materials, has received much less attention and the field is still in its infancy. To date, AM of magnetocaloric regenerators for magnetic refrigeration (an energy-efficient alternative to the conventional vapor-compression cooling technology), remains a challenge. There are several magnetic refrigerator device designs in existence today that are predicted to be highly energy-efficient, on condition that suitable working materials can be developed. This challenge in manufacturing magnetocaloric devices is unresolved, mainly due to issues related to shaping the mostly brittle magnetocaloric alloys into thin-walled channeled regenerator structures to facilitate efficient heat transfer between the solid refrigerant and the heat exchange fluid in an active magnetic regenerator (AMR) cooling device. To address this challenge, we explore the possibility of using extrusion-based additive manufacturing (AM) for 3D printing magnetocaloric structures in this work.

Nominal compositions of $\text{LaFe}_x\text{Co}_y\text{Si}_{13-x-y}$ alloys were used for this investigation. The effects of extrusion printing on the composition were evaluated by microstructural, crystal structure, and magnetic characteristics probing. Chemical stability of precursor powders was assessed by simulating partial in-operando conditions of an Active Magnetic Regenerator (AMR) setup where heat transfer fluid (DI water) was circulated through the magnetocaloric structure with the aid of a circulating rig. 3D printed parts were immersed in a beaker setup with room temperature tap water (300ml) placed on a magnetic stirrer to simulate flow. Results were presented as comparisons of precursor powders and 3D printed scaffold in terms of composition as well as magnetic properties. X-Ray Diffractometry (XRD) data showed no changes in the composition of the 3D printed samples with similar amounts LaFeCoSi and $\alpha\text{-Fe}$ phases present in the structure. Immersed samples of precursor powders showed introduction of Fe_3O_4 oxide phases where higher compositions of oxide were seen for samples of longer immersion. Magnetometry data showed degradation of magnetocaloric response in polymer blended 3D printed structures with a ΔS_{mag} decrease of 35% and lowered saturation magnetization (M_s). Water immersed precursor powders showed gradual degradation of ΔS_{mag} for longer immersion times as well as lowered M_s with no changes in the curie temperature (T_c) among all the samples. Broadly speaking, this work demonstrated the printability of the magnetocaloric material into a functional regenerator type structure and the poor chemical stability of $\text{LaFe}_x\text{Co}_y\text{Si}_{13-x-y}$ alloys.

Chapter 1

Introduction

1 Introduction

1.1. Energy Consumption

During the post-industrial revolution era, various fronts of the world economy became dependent on heavy machinery that utilized the conversion of fossil fuel and, more recently, renewable energy to power their operations. As we progress towards sustainable energy, it is important to consider the tradeoffs due to the prolonged dependence on non-renewable energy. One of these tradeoffs is the sustainability of newer technologies. Indeed, data collected in 1973 showed that coal, oil, and natural gas made up more than 75% of the global energy supply share, while the rest of the contributions came from nuclear, biofuel, and hydropower. By 2019, these numbers skewed more to the renewable energy side with a growth of almost 10% across the board [1]. 45% of the consumption was at residential units. This number continues to grow as real estate grows to accommodate the growing population. However, most residential units utilize non-renewable energy for power, where 70% of the energy is used up in refrigeration systems [1]. Given this, it is important to consider alternative methods for refrigeration.

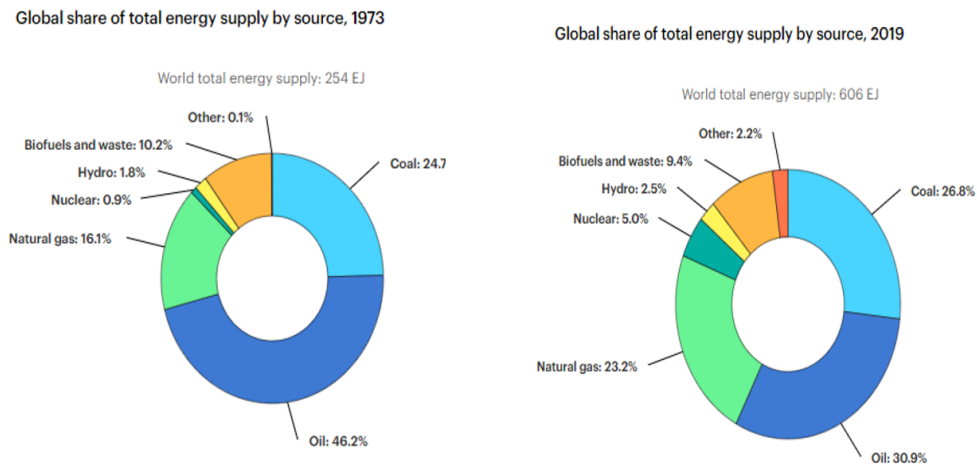


Figure 1: Global share of total energy supply by source in 1973 (left) and 2019 (right) [1]

1.2. Current Refrigeration Technology

Vapor-compression refrigeration systems in which the refrigerant undergoes a phase change, is the most widely used method for domestic refrigerators and air-conditioning systems in buildings and automobiles. Vapor-compression cooling uses a circulating liquid refrigerant (most commonly R134a, also known as Freon), as the medium which absorbs and removes heat from the space to be cooled and subsequently rejects that heat elsewhere. Figure 2 depicts a typical, single-stage vapor-compression system. All such systems have four components: a compressor, a condenser, a metering device or thermal expansion valve, and an evaporator.

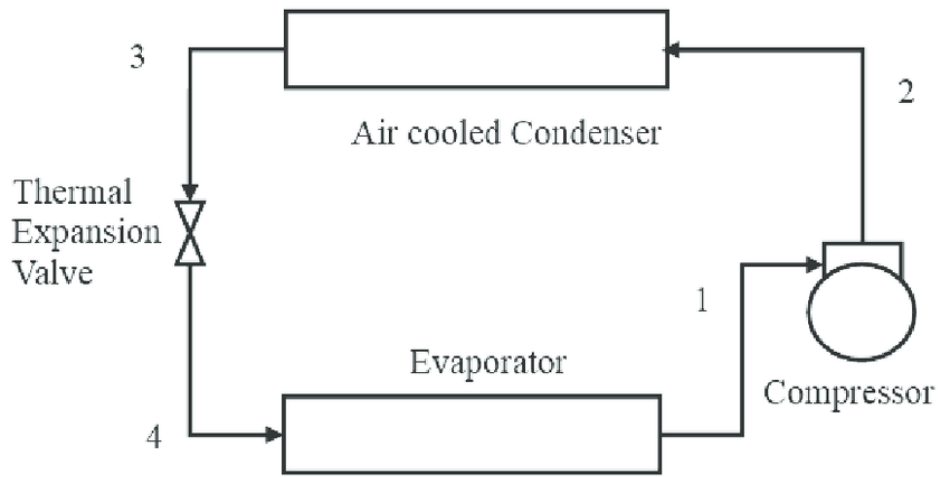


Figure 2: Vapor Compression Cycle [2]

Circulating refrigerant enters the compressor in the thermodynamic state known as a saturated vapor and is compressed to a higher pressure, resulting in a higher temperature as well. The hot, compressed vapor is then in the thermodynamic state known as a superheated vapor and it is at a temperature and pressure at which it can be condensed with either cooling water or cooling air flowing across the coil or tubes. The superheated vapor then passes through the condenser where heat is transferred from the circulating refrigerant to an external medium, allowing the gaseous refrigerant to cool and condense into a liquid. The rejected heat is carried away by either the water or the air, depending on the type of condenser. The condensed liquid refrigerant is next directed to an expansion valve where it undergoes an abrupt reduction in pressure. That pressure reduction lowers the temperature of the liquid and vapor refrigerant mixture to where it is colder than the temperature of the enclosed space to be refrigerated. The cold refrigerant liquid and vapor mixture is then routed through the coil or tubes in the evaporator where air in the enclosed space circulates across the coil or tubes due to either thermal convection or a fan. Since the air is warmer than the cold liquid refrigerant, heat is transferred which cools the air and causes evaporation of the liquid, returning it to a saturated vapor state. To complete the refrigeration cycle, the refrigerant vapor from the evaporator is routed back into the compressor [3].

Freon technology, according to the U.S. Energy Information Administration, consumes up to 1.28 quadrillion BTU per year [4]. The current cooling technology has its drawbacks in many distinct aspects. The main issue with the sustainability of such a technique is its immense effect on pollution. More specifically, it releases harmful chemicals such as hydrofluorocarbons (HFCs) and Chlorofluorocarbons (CFCs) into the environment through leaks in the system. HFCs and CFCs are known chemicals that can interact with our atmosphere's ozone layer and can deplete the surface, exposing the world to the harmful

rays emitted from the sun. This alone can be a huge factor in our decision to look for alternative methods for refrigeration.

1.3. Alternative methods for refrigeration

Conventional refrigeration methods have harmful effects to the environment and are not sustainable as a long-lasting technology. New methods have been developed through the years that had their advantages over conventional methods while bringing about their own shortcomings. Prominent among these alternatives are thermoelectric, thermoacoustic, and caloric cooling techniques.

Thermoacoustic refrigeration utilizes pressure change in acoustic waves to mediate heat transfer between two reservoirs at different temperatures [5]. When parcels of gas in a sound wave are adiabatically expanded and compressed, they will cause a change in the pressure, which can incur a temperature change. A loudspeaker can be used to generate these sound waves that can be either standing or traveling waves, depending on whether a resonator or a regenerator is used. A resonator uses the idea that two wave sources will be placed opposite each other and create interference between them as they travel in opposite directions, creating resonance and a standing wave. A stack is placed inside of the resonator field, a temperature differential is created, where heat exchangers can be placed on either side of it to move the heat.

Thermoelectric coolers rely on the thermodynamically reversible Peltier effect. An applied DC provides the work input needed to drive charge carrier (electrons and holes) diffusion in an electrically conductive material [6]. This causes heat to flow from one junction of two dissimilar conductors to the other junction. Work on thermoelectric technology began in the early 1800s, when Thomas Seebeck discovered thermoelectricity and progressed to the point where commercial products were produced [7]. It is the only cooling concept evaluated in this assessment with commercial products, but current application is limited to niche markets, where other attributes outweigh its low efficiency and relatively high cost. Opportunities for performance improvement exist by implementing available semiconductor materials with more than double the performance of commonly employed materials. However, even utilization of the best available thermoelectric materials would not result in a device as efficient as the best currently available vapor compression equipment. Thus, the overall prospect for this technology is rated “fair”.

Magnetic cooling utilizes the application of an alternating magnetic field to cool ferromagnetic materials via the magnetocaloric effect [8]. The application of a magnetic field heats the material under adiabatic conditions. Rejection of this heat to the environment, followed by removal of the magnetic field, cools the material below its initial temperature. The cooling load may then warm the cooled material, completing the cycle. Thermodynamic modeling suggests that magnetic cooling could have a 25% efficiency advantage over the best current vapor compression technology in air-cooled applications [9]. Although prior federal

funding of this concept did not result in a commercial product, recent advances in magnetocaloric materials and widespread international interest make magnetic cooling a “good” prospect worthy of additional federal funding. As worthy as this technology of investigation, this study will look into this technology in terms of its feasibility.

Chapter 2

Magnetic Cooling

2 Magnetic Cooling

2.1. Overview of Magnetocaloric Technology

Magnetocaloric materials, or MCMs, are compounds that exhibit a magneto thermodynamic phenomenon known as the magnetocaloric effect (MCE) when subjected to a magnetic field [8]. The development of these materials is mainly due to the rise of the magnetic refrigeration (MR) technology, which has brought an alternative to the conventional gas compression techniques. When the magnetic field is applied to a magnetic material, atoms will reorient their magnetic moments. When this process is undergone adiabatically (no gain/loss of heat), there will be an increase in the temperature and subsequently decrease as the magnetic field is removed.

To characterize a magnetocaloric material, there are several relevant parameters that need to be experimentally determined. The most intuitive one is the adiabatic temperature change, ΔT_{ad} , which is the temperature change of the material when adiabatically magnetized/demagnetized. Less obvious, but easier to determine experimentally is the magnetic entropy change (ΔS_{mag}) of the system [10]. As temperature changes in a magnetocaloric material are due to changes in the order of magnetic moments, it is intuitively understood that materials with large ΔS_{mag} values are likely to be good candidates for magnetic refrigerants. Change in entropy of a magnetic system is related to the magnetization of the material with respect to the temperature [8]. This relationship is stated in the Maxwell relation:

$$\left(\frac{\partial S}{\partial H}\right)_T = \left(\frac{\partial M}{\partial T}\right)_H$$

Given the temperature and magnetic field dependence, the magnetic entropy change is then calculated by:

$$\Delta S_M(T, H) = \int_0^H \left(\frac{\partial M(T, H)}{\partial T}\right)_H dH$$

The MCE varies for different materials and is dependent on temperature and the strength of the magnetic field applied for a given material. The magnetocaloric effect is usually strongest in the vicinity of a magnetic phase transition temperature (referred to as the Curie temperature T_c in the case of a ferromagnetic (FM) \rightarrow paramagnetic (PM) transition) [11]. The application of magnetocaloric effects date back to 1917 when scientists P. Weiss and A. Piccard first discovered Nickel to have a reversible heating capacity of Nickel [12]. Later in 1933, MacDougall introduced the first ever low temperature magnetocaloric material in Gd₂(SO₄) paramagnetic salt which had a cold temperature value of around 0.25K [13]. The application

of low-temperature MCM materials seemed to be impractical, therefore, it was necessary to develop materials that operated in room temperature conditions⁷.

The first room-temperature magnetocaloric material was developed in the 1970s when Brown reported ferromagnetic Gadolinium working material which was subjected to 50 cycles inside of a field. This system subsequently reached a low temperature of 47K, which led to the discovery of an Active Magnetic Refrigeration system (AMR) [14]. This system was designed to act as a heat source/sink to transport energy from the magnetocaloric material through a heat exchanger type of medium. When an external magnetic field is applied to the magnetocaloric material placed inside the thermally insulated system, adiabatic demagnetization of the material occurs. This leads to an increase in temperature of the material, which acts as a heat source that is later then expelled through a heat exchanger. To prevent any further changes in the magnetic ordering of the system, the magnetic field is kept relatively constant in an isofield cooling process. After the heat is released through the heat exchanger, the magnetic field is removed to keep the entropy change constant, decreasing the temperature of the material. The cycle will keep repeating itself after said step as an isofield heating process is applied to prevent any further increase in the magnetocaloric material and is kept at an equilibrium temperature as the heat load [14].

The knowledge of the magnetocaloric effect and its potential uses were mostly theoretical till the 1990s when Ames Laboratories, a US DOE lab, and Astronautic Corporation of America first unveiled a working prototype of a cooling technology which consisted of a room temperature magnetocaloric material [15]. Since then, multiple efforts have been devoted to two different research purposes: (1) understanding the physical phenomenon that actuates the exceptional functional response of commercially viable magnetocaloric materials and the materials that have already been tested but have been deemed not feasible for system integration and (2) developing laboratory/pre-industrial grade magnetic refrigeration prototypes. Material systems such as $\text{La}(\text{Fe}, \text{Mn}, \text{Co}, \text{Mn})_{13-x}\text{Si}_x(\text{H}, \text{N}, \text{C})_y$, Fe_2P -type compounds (MnFePSi), Ni-Mn-based Heusler, AlT_2B_2 ($\text{T}=\text{Fe}, \text{Co}, \text{Ni}$) borides, and $\text{La}_{1-x}\text{Ca}_x\text{MnO}_3$ manganite have proven to have magnetocaloric effects that are of significance in a laboratory testing stage, however have limitations that prevent them from scaling up to a prototype device with current technology and knowledge [16].

The heat exchanger is a very important component of the system. The amount of heat that is transferred as well as the overall efficiency of the system highly depends on the overall quantity of the heat exchangers. The quantity depends on several factors, including the physical properties of the fluid, the fluid flow pressure, the porosity of the working magnetocaloric material, the frequency of the magnetocaloric material component in both the rotary and reciprocating designs, etc. [17].

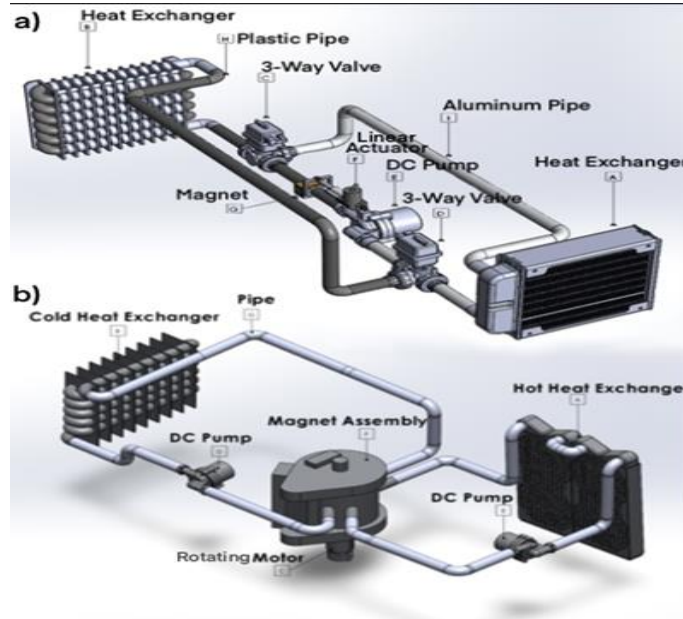


Figure 3: Magnetic Regenerator System Design working in a) Reciprocating Magnetic Field and b) Rotary Magnetic Field [18].

2.2. Challenges Toward System Integration

The nature of magnetocaloric heat transfer requires the presence of a heat transfer fluid as well as a certain configuration of the material itself to allow for the heat exchange fluid to pass through the medium to accomplish successful heat transfer. With that comes certain limitations that restrict the development of such devices to attain maximum performance. Some of the biggest challenges that come with the design of these devices and their integration towards a bigger functional system are mechanical and chemical stability of the magnetocaloric material due to the nature of their structure.

Magnetocaloric structures are devised such that their microstructure can allow for a heat transfer fluid to pass through it. In an active magnetic regenerative device, the magnetocaloric material is immersed in a heat exchange fluid whose selection is driven by various factors such as good heat transfer characteristics, low viscosity, thermal and physical property stability across the working temperature of the material as well as environmental friendliness [16] [19]. Figure 4 displays the number of prototypes that have been made to date utilizing heat transfer of specific fluids. To achieve maximum convective heat transfer from or to the fluid, the magnetocaloric material should be shaped such that it provides the maximum amount of heat transfer area. When the principles of heat transfer are considered, the Nusselt number of the flow of a heat transfer fluid is directly related with the heat transfer coefficient and the thermal conductivity and inversely proportional to the characteristic length of the fluid channel [19]. Therefore, it is very necessary to consider the fact that the porosity of said magnetocaloric material depends not only on the macroscopic properties

of the working material but also on the fluid properties. These fluids also have the capability of causing chemical instability issues on the working materials in the form of corrosion and aging. Corrosion processes in magnetocaloric devices can have complex mechanisms, which can lead to multiple forms of localized corrosion such as pitting, crevice and galvanic corrosion. Inhibition methods of these corrosive tendencies of the materials require specific processing techniques that can eliminate the effects of corrosion and prolong the lifetime of the working material.

For gaseous heat transfer fluids such as air or helium, a high porosity is necessary to effectively transfer heat [20]. However, shaping the working magnetocaloric materials such that their porosity is high can present different challenges to the overall design. One glaring issue that comes with it is the mechanical stability of the material. Highly porous designs tend to have lower mechanical strength and general stability as their particles tend to be much more sporadically placed in the structure [21]. Microchannels are a solution to alleviate the effects of porosity on the mechanical stability of structures without sacrificing the overall accommodation of heat transfer channels in the system [19]. However, solid processing techniques that allow for the formation of microchannels can be highly complicated to achieve desired properties. As seen in Figure 4, magnetocaloric materials can be formed into packed powder beds were crushed, unshaped or gas atomized particles can be used to form the bed with minimal amounts of polymer mass fractions (<5 wt%) added as a binder, or into periodically ordered structures such as stacked plates, circular or honeycomb microchannels. These structures, specifically the periodically ordered structures, require very meticulous processing techniques that are impractical for large industrial level production of these regenerators.

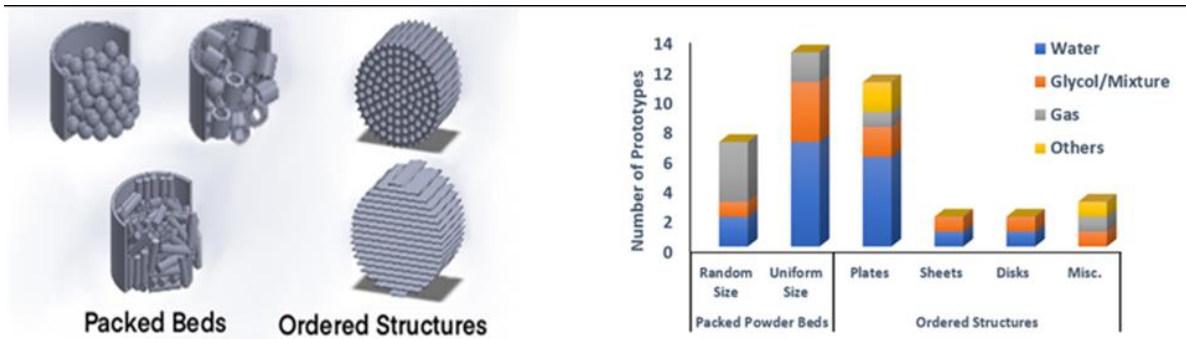


Figure 4: Different conformations and Shapes of Magnetocaloric Regenerators (left) and Statistical distribution of heat exchange fluids and architectures of materials used to fabricate magnetocaloric regenerator prototypes (right) [18]

2.3. Problem Statement

Magnetocaloric materials can be processed to take on granular type powder shapes that can be formed into packed beds with different particle shapes or into orders structures that can provide microchannels for heat

transfer fluid flow. Regardless of the magnetocaloric structure form, MCE will be induced on the system subjected in a magnetic field. However, magnetic response of a magnetocaloric structure will vary depending on the specific form of the material.

Packed particle beds or stacked plates can be formed and separated by spacers to create channels for heat transfer [22]. However, these processing techniques present a challenge to the overall heat transfer efficiency of the magnetocaloric system. Packed powder beds tend to have sites of segregation and sedimentation which can result in pressure drop of the heat transfer fluid across the length of the regenerator path [23]. In plate-like structures, the application of subtractive manufacturing methods such as drilling or forming techniques do not provide sufficient flexibility in terms of the required sizing and geometry for an effective heat transfer path. Further, these regenerator plates will usually consist of a caloric powder and polymer binder to alleviate issues arising from mechanical brittleness [23]. The use of binder polymer in a system requires lower caloric powder to be used which dilutes the caloric response and decreases the thermal conductivity. Therefore, microchannel geometries which can be shaped into various cross sections are a much more practical solution for heat transfer path [23]. Conventional subtractive manufacturing methods such as milling, and drilling do not present an active solution to the overarching issue of designing microchannels as these processes do not possess the necessary tools to control the design of the internal structure.

Additive manufacturing is a much more attractive approach to tackle the problems with intricate geometry design. Processing techniques such as Powder Bed Fusion (PBF) and Direct Energy Deposition (DED) provide greater control over geometry construction and said microchannel architecture [24]. However, such approaches use high energy sources which require expensive infrastructure. In addition, compositional inhomogeneity as well as phase stability issue can arise because of these techniques do to the melting and recrystallization of the magnetocaloric particles during shaping [25]. Extrusion-based 3D printing is an optimal method of shaping functional magnetocaloric regenerators. Improved resource efficiency and better quality of product are among some of the upsides of using extrusion-based printing techniques. Layer by layer deposition of said magnetocaloric materials allows for intricate geometries and better control on the microstructural formation of the regenerators [26]. The caveat that comes with extrusion-based printing techniques require the presence of a sacrificial binding agent, usually in the form of a polymer. It is important to note that the volume of polymer used in a given magnetocaloric material is very small, which provides for a more sustainable and environmentally friendly manufacturing technique.

This study explores the printability of polymer blended $\text{La}(\text{Fe}_{0.842}\text{Co}_{0.073}\text{Si}_{0.084})_{13}$ magnetocaloric alloys and compares the structural, magnetic and chemical stability properties of precursor $\text{La}(\text{Fe}_{0.842}\text{Co}_{0.073}\text{Si}_{0.084})_{13}$ powders and the corresponding 3D printed parts are examined. To explain the rationale of materials

selection, Table 1 provides a quantitative comparison of the magnetocaloric response of these state-of-art materials, as described by the following figures of merit: (i) magnetic entropy and adiabatic temperature change observed upon application of a magnetic field (ΔS_{mag} and ΔT_{ad} , respectively); (ii) thermal conductivity (κ) and (iii) specific heat capacity (C_p). It is obvious that among the state-of-the-art magnetocaloric alloys, $\text{La}(\text{FeSi})_{13}$ based alloys show the magnetocaloric response. The material chosen for this study consisted of a Lanthanum Iron Silicide alloy with Cobalt substitution. Nominal composition of $\text{La}(\text{Fe}_{0.842}\text{Co}_{0.073}\text{Si}_{0.084})_{13}$ was synthesized and obtained by Ames Laboratory, an entity under the US Department of Energy.

Table 1: Comparison of attributes of state-of-the-art magnetocaloric alloys [27] [28] [29] [30] [31]

| | Gd ₃ Si ₂ Ge ₂ family | La(FeSi) ₁₃ family | LaMnO ₃ manganites | NiMn-based Heuslers | MnFeP-type compounds |
|--|---|----------------------------------|----------------------------------|------------------------|-------------------------|
| ΔS_{mag} @ 2T (J/KgK) | 8-14 | 6-22 | 3-5 | 8-12 | 20-25 |
| ΔT_{ad} @ 2T (K) | 5-8 | 2-6.5 | <1 | 2-5 | 2-4 |
| Thermal Conductivity (Wm ⁻¹ K ⁻¹) | ~5-6 | ~8 | ~1-2 | 2 | 4 |
| Specific Heat Capacity @ 2T (JKg ⁻¹ K ⁻¹) | 124-300 | 1000-1500 | 117-250 | 1000-2000 | 1500-1800 |

Chapter 3

Experimental Methods

3 Experimental Methods

3.1. Powder Sample Preparation

20g of the alloy powder was prepared by arc-melting of the constituent elements under argon atmosphere on a water-cooled Cu-hearth. The ingot was re-melted four times, being turned over each time to achieve homogeneity. The total measured weight loss was less than 0.5 wt. %. The as-cast ingot was broken into smaller pieces wrapped in a tantalum-foil, sealed inside a fused-silica tube under vacuum, and annealed at 1050°C for one week, followed by quenching in ice-cold water. Powders from the annealed pieces were prepared by crushing and grinding in an agate mortar with an agate pestle inside an argon-filled glove box and screened to particle sizes of 100 μm and below.

The arc melting process consisted of a vacuum arc melting chamber that was first evacuated to create a vacuum filled with argon gas. The heat that is generated by the electric arc struck between the electrode, and the metal melts the material placed in the crucible to form the alloy. 20 grams of the alloy in stoichiometric proportions were melted together in the water-cooled Cu-hearth which was then remelted four times to achieve homogeneity. The annealing process was done at above recrystalline temperature for a certain amount of time and consisted of a recovery, recrystallization, and grain growth stages. To avoid any type of oxidation taking place after the high-temperature heat treatment, a mixture of hydrogen and nitrogen gas was allowed to flow in the annealing chamber, which was also a method of scaling prevention. The crushing and milling process was used to grind, homogenize, and blend the pure materials in the system. Mortar and pestle that was made up of agate was used to crush the material by pressing hard and rotating and grinding to provide the desired powder form. The annealed pieces were crushed inside an argon-filled glove box and sieved to a uniform particle size of 100 microns and below. A ball mill was then used to grind the samples into 0.2 to 10g of dry brittle samples. Details regarding the powder preparation process is also available in Ref [32].

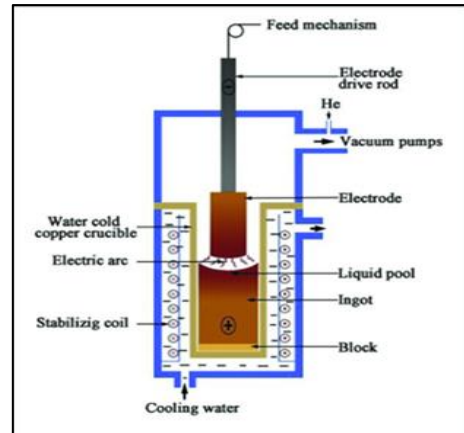


Figure 6: Arc Melting Process [49]



Figure 5: Milling Apparatus

3.2. 3D Printed Sample Preparation

The printing procedure was carried out on an EnvisionTec 3D-Bioplotter at Zhao Lab located in Virginia Commonwealth University. Polyethylene Oxide (PEO) was used as a binder agent in the printing ink. It is a polymer that is usually used for bioprinting processes due to its high molecular weight as well as inert properties. It is also a relatively easy material to thermally degrade at around 330°C for any future high temperature solidification processes. The ink formulation also consists of the addition of three different solvents. Dichloromethane was used as the high volatility solvent to help with precipitation and dissolving of the PEO polymer. Ethylene Glycol Butyl Ether was used as the low volatility solvent with nominal traces in the structure used for fusion of the layers during the printing process. The third solvent used was small amounts of Dibutyl phthalate which helped alleviate the brittle nature of the PEO polymer and give more mechanical stability by crosslinking the polymer.

Once the ink was prepared, it was loaded into printing cartridges with 65 vol% LaFeSiCo-PEO links with 600 μm nozzles. The cartridges were then loaded into a EnvisionTec 3D-Bioplotter that has printing speeds varying from 1-10mm/s depending on the extrusion pressure. Since the ideal thermal transport of the magnetocaloric structure depends on the porosity and surface density, the microchannels were designed in accordance with the surface density of the ink material and the retention of micro-porosity after the printing process. The structural design was created in a CAD software which was sliced for the specified nozzle diameter and then uploaded into the EnvisionTec software. Optimizations on the printing method were done according to the rheology needs of the ink which determined factors such as printing speed, nozzle offset and pressure.

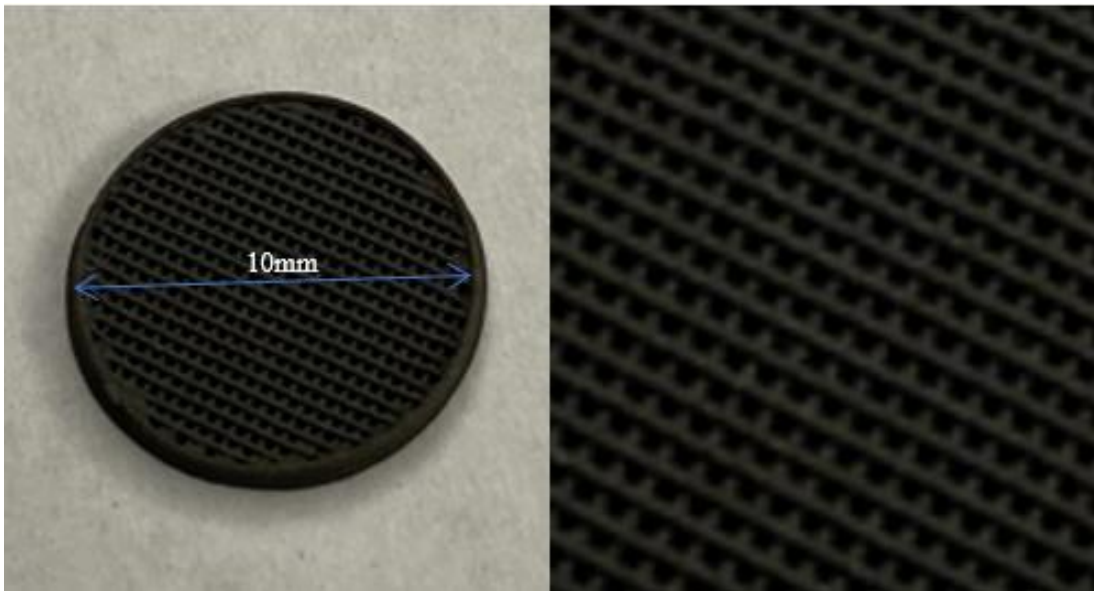


Figure 7: Geometrical visualization of printed LaFeSiCo structures

3.3. Characterization Methods

3.3.1. Scanning Electron Microscopy

Scanning Electron Microscopy is a topical characterization method that uses electron-sample interactions to give information about a sample's morphology, chemical composition, and crystalline structure or orientation of the materials making up the composition. Some of the essential components of an SEM are the electron gun, lenses, sample stage, and detectors for all signals of interest.

High kinetic energy electrons that are accelerated by the electron gun onto the surface of the sample where the electrons collide with the sample's lattice structure and dissipate their energy into various signals produced by electron-sample interactions decelerate in the solid sample [33]. The signals are composed of secondary electrons, back scattered electrons, diffracted backscattered electrons, photons, visible light, and heat. The system utilizes secondary and backscattered electrons as a means of imaging samples. Backscattered electrons are a result of a reflection from the sample by elastic scattering. They have higher energies than secondary electrons, therefore are used to get images that emerge from deeper locations of the sample, consequently giving lesser resolution images than that of secondary electron images. They can provide information about distribution of the various elements in a material system. Since the beam of electrons are very narrow, SEM images have a very large depth of field, giving a very informative 3-dimensional appearance useful to understand the topical structure of a sample [33].

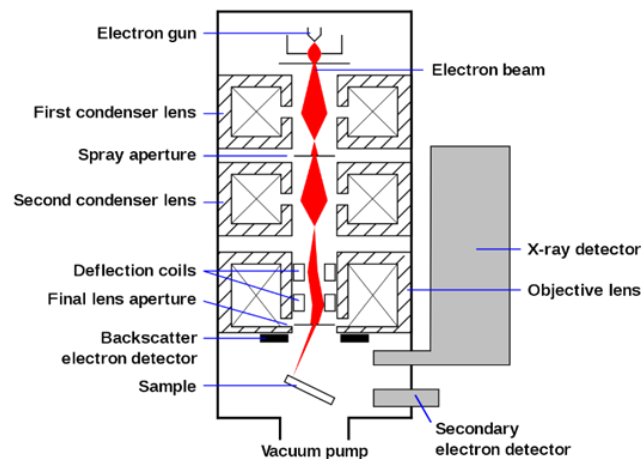


Figure 8: Working Principle of a SEM [33]

3.3.2. X-Ray Diffraction

Another fundamental technique of surface characterization is the use of X-Ray diffractometry. It is a method of rapid analysis primarily used for phase identification of a crystalline material that can also provide unit cell information. In 1912, Max Van Laue discovered that crystalline substances could act as three-dimensional diffraction gratings for x-ray wavelengths like the spacings of planes in a crystal lattice [34].

The technology uses constructive interference of monochromatic x-rays generated by a cathode ray tube and the crystalline sample [35]. The interaction between the incident rays and the sample produces a diffracted ray when the conditions of Bragg's law are satisfied. Bragg's Law states the relationship between the wavelength of electromagnetic radiation to the diffraction angle and the lattice spacing in the crystalline sample [36]. Bragg's Law is governed by the relation: $n\lambda = 2d\sin(\theta)$, where n is the diffraction order, λ is the wavelength of the x-rays, d is the atomic spacing while θ is the incident angle at which the x-rays hit the sample surface.

The intensity of diffracted x-rays is continuously recorded as the sample and detector rotate through their respective angles. A peak, or a sharp spike in the background, occurs when the material contains lattice planes with d-spacings appropriate to diffract x-rays at that angle or incident rays [37]. The results of the diffractometry are plotted on an x-y graph where the intensity of the ray is displayed as peak height as shown below. The diffractometry data collected for the LaFeSiCo samples was done so by using a PANalytical XPertPro diffractometer which uses Bragg-Brentano method of diffraction where incident rays directly display the Bragg peaks of the crystal structure

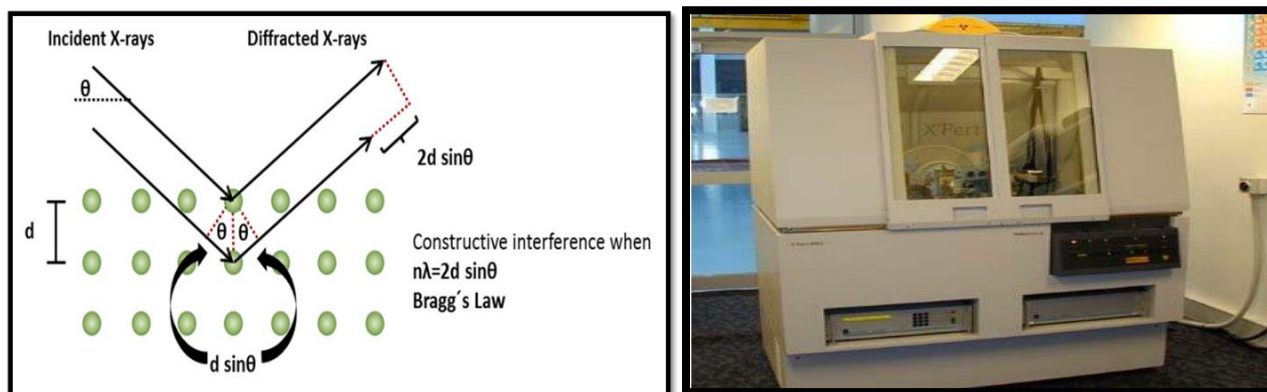


Figure 9: Working Principle of X-Ray Diffractometry [35] and Panalytical X'Pert Pro Diffractometer [38]

3.3.3. Magnetofunctional Response

Magnetic measurements were conducted on a DynaCool Physical Property Measurement System (PPMS) with a measurement system known as Vibrating Sample Magnetometry (VSM). A VSM is a measurement technique that collects magnetic property data using Faraday's Law of Induction where a sample is placed in a magnetic field and is allowed to vibrate back and forth inside the field. The aligning of the magnetization with the external field is what decides if the sample is magnetic or not. Using a piezoelectric material, the magnetic dipole moment of the sample material creates a time variant magnetic field. The alternating magnetic field source induces an electric field in the pickup coils of the VSM which is then translated into a magnetization curve where the amount of current that is picked up is directly proportional to the magnetization of the material.

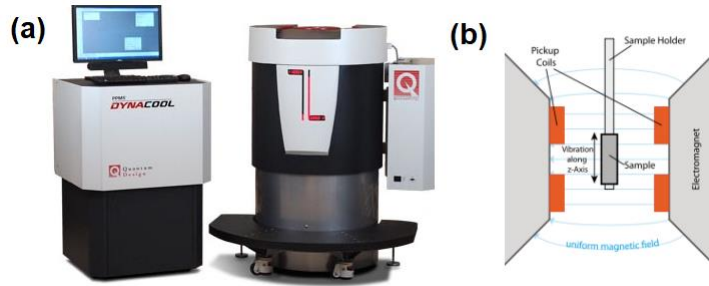


Figure 10: (a) DynaCool Physical Property Measurement System (PPMS) for Vibrating Sample Magnetometry (VSM) [39]; (b) Operating principle of a VSM [40]

Two different types of data can be extracted from this measurement. One is the magnetothermal curves that illustrates the relationship between the varying temperature of the material and the magnetization of the material at a constant magnetic field H (see Figure 10(a)); and the other is the variation of magnetization of a material M for a varying magnetic field strength H at constant temperature T (see Figure 10(b)). As relevant to this thesis, two figures of merit are important, as defined below:

Curie temperature: Permanent magnetism is caused by the alignment of magnetic moments and induced magnetism is created when disordered magnetic moments are forced to align in an applied magnetic field. The temperature above which certain materials lose their permanent magnetic properties and become disordered (paramagnetic) is called the Curie temperature and it is denoted as T_c . In this work, T_c was determined from the inflection point of the M vs. T transition as the maximum of the derivative of M with respect to T (i.e. $(\frac{dM}{dT})_{max}$).

Saturation Magnetization: Magnetic saturation is the state reached when an increase in applied external magnetic field H cannot increase the magnetization of the material further, so the total magnetic flux density H more or less levels off. Figure 10 shows a typical M - H curve of a ferromagnetic material. The saturation magnetization is denoted as M_s .

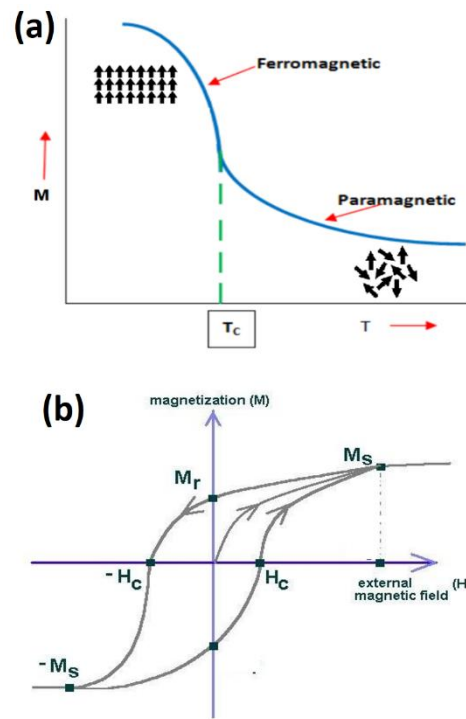


Figure 7. Visual representation of a: Temperature-dependent magnetization curve; (b) Field-dependent magnetization curve [47]

Characteristically, the thermal behavior of magnetocaloric compounds is strongly correlated with the magnetic entropy change (ΔS_{mag}) of the system. In this study, ΔS_{mag} was therefore determined from the Maxwell relation using isothermal $M(H)$ curves measured at temperature intervals of 5 K in the vicinity of the Curie temperature: $S(T, \Delta H) = \int_0^H \frac{\delta M(H, T)}{\delta T} \delta H$. Graphically, the magnetic entropy change is quantified by the difference in integrated area when the temperature of the material is raised by a certain amount between the successive isotherms. The saturation magnetization increases steadily for magnetocaloric materials until the transition temperature near T_c .

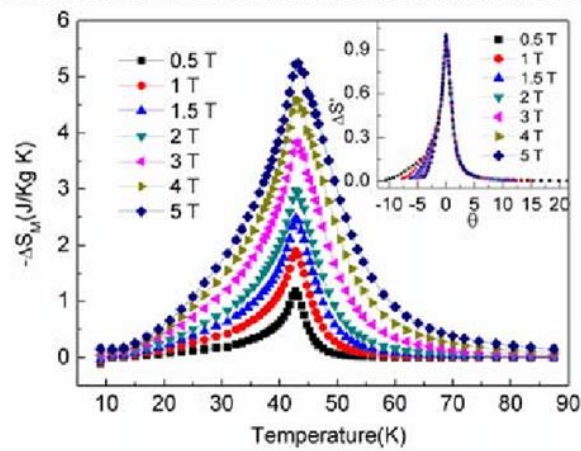


Figure 8: Visual Representation of a Magnetic Entropy Change Curve [41]

3.4. Chemical Stability and Corrosion

Both precursor powder and 3D printed samples were subjected to varying periods of water immersion to test for chemical stability analysis. Powder samples were placed in resin bags of <15 microns in a water flow simulating rig as displayed in Figure 12. The sample bags were placed in each of the three capsules carved out of the PVC pipe and tied at the top with a nylon string. Deionized water was made to flow through the pipe channel and subsequently the sample bags to simulate an erosive flow through the sample. The samples were taken out of the flow one by one in intervals of 7 days and studied for chemical stability to evaluate the effects of fluid flow on the magnetocaloric structure as a function of time.

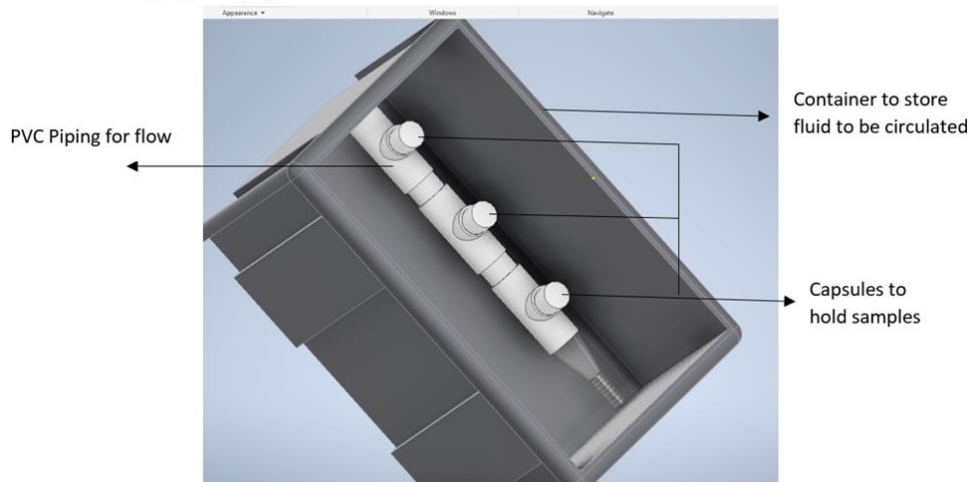


Figure 9: Corrosion Test Rig for powder samples

The 3D printed scaffold had a different setup for its immersion procedure. The corrosion test rig provided issues with the flow control rate as the pump pushing the water had a high-pressure rating which could damage the 3D samples as a result of the high energy flow. As shown in figure 16, the sample was placed in the same 15-micron resin bag which held the powder samples. Tap water was used as an immersion fluid inside of a large beaker where the sample bag tied with a nylon string was placed hanging from a clamp on top of the beaker. The beaker setup was put on top of a magnetic stirrer where the magnetic piece was placed inside at the bottom of the beaker and was allowed to stir at 1000rpm to simulate flow through the resin bags. The sample was immersed inside of the beaker for a period of 3 days as opposed to its powder counterparts which were in immersion for up to 31 days.

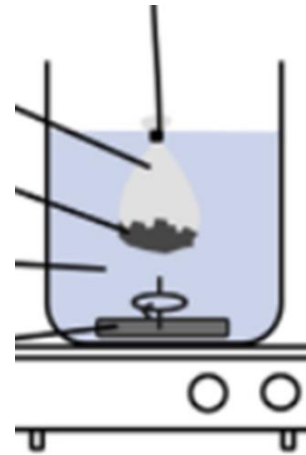


Figure 10. Immersion setup for 3D printed scaffold [48]

Chapter 4

Results and Analysis

4 Results

4.1. Microstructural properties and Composition of Precursor Powders and 3D Printed Samples

As seen in figure 17, precursor powder samples and 3D printed scaffolds of LaFeSiCo were characterized for their crystal structure and phases through x-ray diffractometry done from 2theta values of 30°-130°. Diffractometry data was analyzed for crystal structure as well as phase identification using open-source refinement software “GSAS II”.

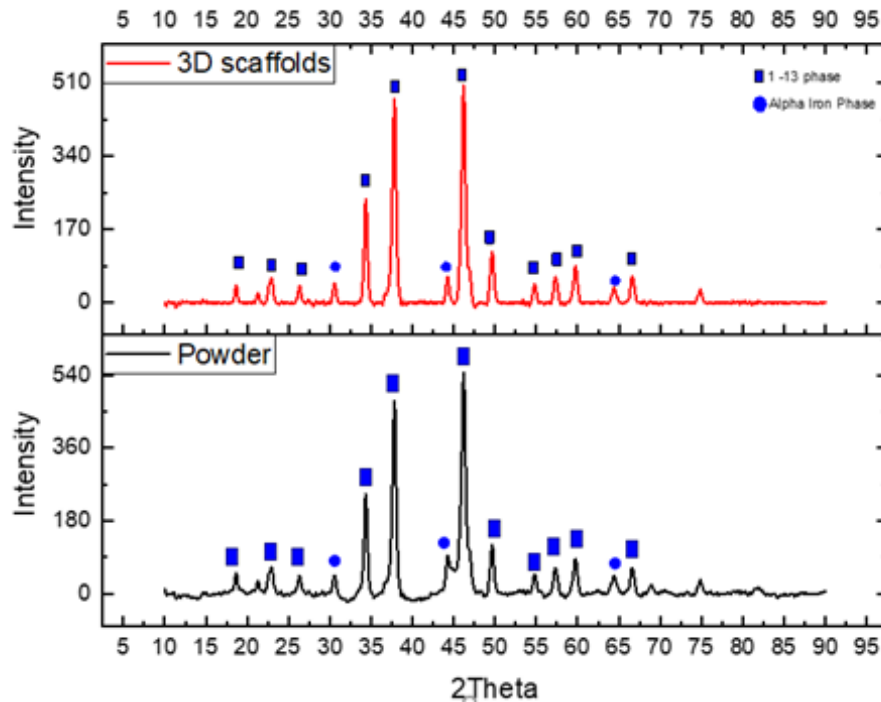


Figure 11: XRD peaks for precursor powders and 3D printed scaffolds of LaFeSiCo Samples

98.3 w.t.% of LaFeSiCo parent compound was identified as the primary phase of the material system with nominal (1.7 w.t%) alpha-Fe phase identified for a Goodness of Fit (GOF) of 1.25. Reflections list show highest intensity peaks at 38.2°, 46.7° for [422] and [531] orientation planes of the LaFeSiCo crystal structure and at 44.7° for the [110] plane of the alpha iron structure. The figure also shows the phase composition as well as Bragg peaks of polymer blended printed LaFeCoSi samples. Bragg peaks of primary LaFeCoSi phase as well as secondary Alpha-Fe phases are observed in the system. Introduction of binding polymer into the structure has not altered the phase composition of the compound as 98 w.t% of the printed material is of the primary LaFeCoSi phase while the rest is attributed to secondary α -Fe phase.

4.2. Magneto functional properties of precursor powders and 3D printed samples

4.2.1. Temperature and Field Dependent Magnetization

Figure 16(a) shows the temperature-dependent magnetization curves measured at $\mu_0H=1000$ Oe for the LaFeSiCo precursor powders and the 3D printed sample. As such the magnetothermal behavior of both samples, shown in Figure 16(a), is comparable. Upon heating at $\mu_0H=0.01$ T, the precursor powders and the annealed 3D printed sample undergo a magnetic transition from ferromagnetic to paramagnetic phase at the Curie temperature of $T_c=299.67$ K, Figure 16(a). Subsequently, during cooling, a paramagnetic to ferromagnetic phase transition is observed at 271.86 K. The thermal hysteresis in the samples, as determined by the difference between the magnetic transition temperature during heating and cooling was calculated as 27.81 K. The field-dependent magnetization measurements of the LaFeSiCo precursor powders and the 3D printed sample indicate a M_s of 130 emu/g and 83 emu/g, respectively. The value of the T_c of the LaFeSiCo samples investigated in this work agrees with literature values of compositions which equals around 300K [32]. The reduction in M_s in the 3D printed samples is attributed to the presence of the polymer binder in the sample.

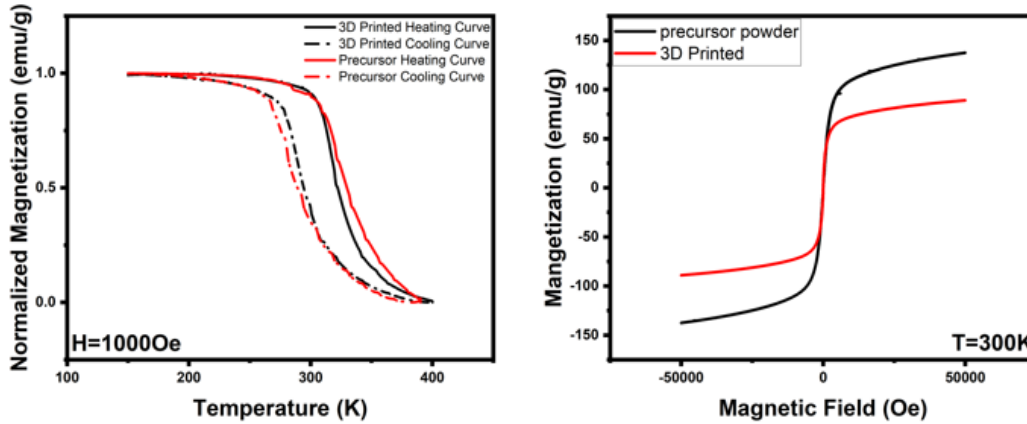


Figure 12: Temperature (0.1T) and Field dependent (300K) magnetization curves for the precursor powder and polymer blended 3D sample

Table 2: Magnetic Properties of the precursor powders and the 3D printed samples

| Material Form | T_c | M_s |
|------------------|--|-----------|
| Precursor Powder | 299.67 (K) Heating, 271.86 (K) Cooling | 130 emu/g |
| 3D Printed | 299.67 (K) Heating, 271.86 (K) Cooling | 83 emu/g |

4.2.2. Magnetic Entropy Change

Figure 17 shows the temperature-dependent magnetic entropy change curves of the LaFeSiCo precursor powders and the 3D printed sample at an applied magnetic field of 3T. The magnitude of the maximum magnetic entropy change ΔS_{\max} ($\mu_0 H = 3T$) of the precursor powders was found to be 7.8 J/kg-K - a value that is slightly elevated from values in previous efforts of investigation of the magnetocaloric response of LaFeCoSi powders [32]. The ΔS_{\max} of the 3D-printed sample, 4.4 J/kg-K, was found to be significantly lower than that of the precursor powders – an observation attributed to two factors: (1) Presence of the polymer binder that dilutes the mass magnetization of the sample; (2) Presence of secondary ferromagnetic phases, namely α -Fe.

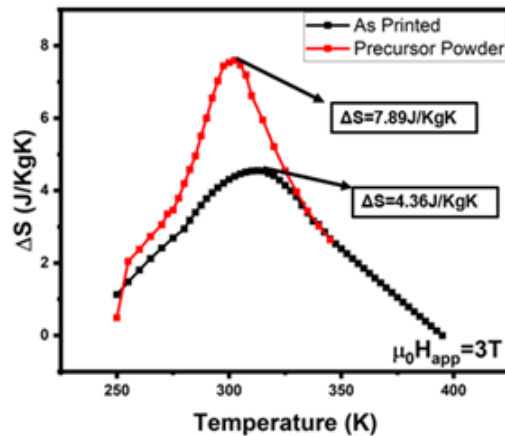


Figure 13: Entropy change of LaFeCoSi powders and 3D printed pieces

4.3. Chemical Stability of Precursor Powders

4.3.1. Microstructure and Phase Compositions of Powders after Immersion in Water

The powder samples and polymer blended 3D samples of LaFeSiCo were both immersed in water to study the effect of heat transfer fluids on the chemical stability of the structures as well as their magneto functional response. X-ray diffraction data is shown in figure 19 for precursor powder samples under immersion and analyzed after being taken out of the water consecutively. The first sample bag's XRD data showed Fe_3O_4 oxide peaks developing in the crystal structure because of oxidation. Consecutive immersion resulted in higher intensity peaks of the oxide peaks where higher amounts of oxides are appearing in the structure as seen with the 14-day, 21-day and then 31-day peaks. Peaks of the secondary α -Fe phase decrease substantially after 21 days, which indicates the formation of Fe_3O_4 in the composition is due to the oxidation of alpha iron molecules. The overall intensity of the peaks decreases as more oxidations occurs inside of the material. Peak width is also seen to be slightly less as immersion time increased from 7 days onwards. Peak width is an indication of lattice size. A decrease in the peak width means the lattice sizes are bigger,

which is supported by the oxide formations that have higher lattice parameters than that of the primary LaFeSiCo and alpha-Fe phases in the system. There were no other phases that were to be expected due to oxidation (LaO, Fe₂O₃) present in the composition

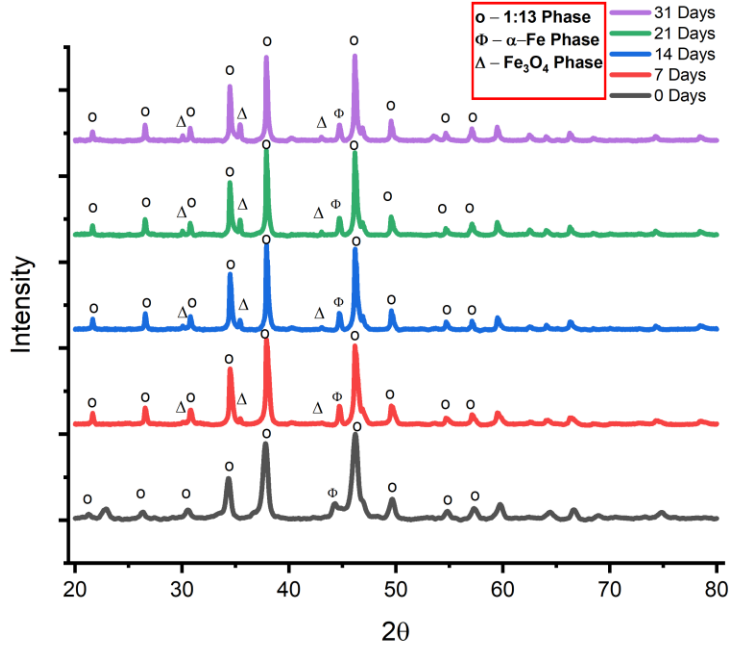


Figure 14: Bragg peaks of LaFeCoSi precursor powders immersed in deionized water for up to 31 days

4.3.2. Magnetofunctional Response of Immersed Precursor Powders

Magnetic measurements of immersed LaFeSiCo powders indicate degradation in the magnetic properties of the powders over time, as seen in Figure 19. M vs. T plots show a gradual decrease in the steepness of the transition at for both the heating and cooling curves over time. This is a result of the introduction of oxide formation in the material system limiting the magnetization of the parent LaFeSiCo material. Since sharper drops in the transition are indication of second order transition behavior, it can be inferred that introduction of the oxide phase in the material dampens the reversibility of the magnetic material. This is also supported by the M vs. H plots where field dependent magnetization of the material degrades over time by the gradual reduction of the saturation magnetization over time. Higher M_s is seen for the samples that were immersed for 21 days than that of their 7 day and 14-day counterparts. The reasons for this are unclear as the general trend followed by the magnetic entropy change and field dependent magnetization curves is that magnetization decays over longer periods of immersion.

The magnetic entropy change curves of the samples show a minor reduction in the magnetic entropy change going from 7 days to 14 days. However, a significant decrease in ΔS is seen after 21 and 31 days of

immersion. Since the basic assumption is that magnetic performance decreases as more La-rich phases and Alpha Iron phases are oxidized, magnetic entropy decrease is also attributed to this reaction. However, as seen by the magnetization curves for the 14-day samples, significant oxidization does not seem to occur till around midway between 14 days and 21 days of immersion where large amounts of La-rich and alpha Fe phases are oxidized. This also further proves the theory that oxidation happens at a faster rate when lower amounts of alpha-Fe phases are present in the material as those phases oxidize and create the Fe_3O_4 phase which was seen in high amounts in the XRD reflections

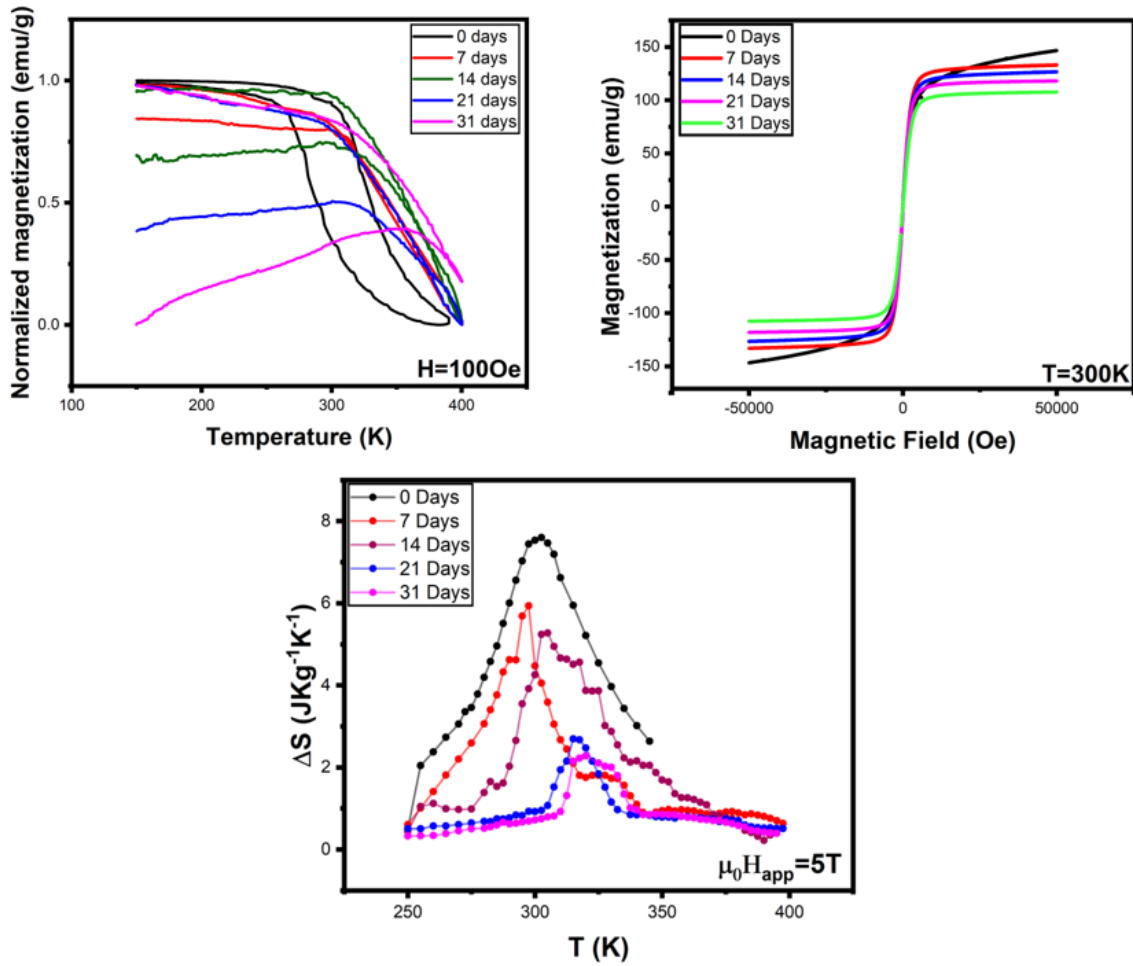


Figure 15: M-T, M-H and ΔS_{mag} curves of water immersed samples

Table 3: T_c , M_s , and ΔS comparisons of immersed and non-immersed precursor powders

| Powder Immersion Time | T_c (K) (0.01T) | M_s (emu/g) (250K) | ΔS (J/Kg*K) |
|------------------------------|-------------------|----------------------|---------------------|
| 0 Days | 300 | 145 | 7.83 |
| 7 Days | 297 | 135 | 5.78 |
| 14 Days | 297 | 119 | 5.14 |
| 21 Days | 296 | 110 | 2.33 |
| 31 Days | 296 | 107 | 2.04 |

4.4. Chemical Stability of 3D Printed Samples

During extrusion-based additive manufacturing, the magnetocaloric powders were blended with Polyethylene Oxide PEO to facilitate net shaping and to improve the mechanical stability of the 3D printed part. PEO is hydrophilic [42] and therefore not surprisingly, when subjected to the flow system shown in Fig 13, the polymer dissolved and the integrity of the solid structure of the sample was compromised.

It is surmised that going forward, the extrusion-based 3D printing process must be re-designed to incorporate a hydrophobic polymer. Alternatively, PEO may be removed from the composite system through a carefully designed heat treatment protocol, as show in recent studies. Research efforts to this end are currently ongoing at the AM²P Lab at Virginia Commonwealth University.

Chapter 5

Conclusion

5 Conclusion

5.1. Summary

Previous investigations on manufacturing processes to produce magnetocaloric regenerators have provided insight on the potential advantages and drawbacks of using specific methods on geometry design and formability. Powder extrusion processes that were utilized on a slightly different composition ($\text{La}_{0.7}\text{Ce}_{0.3}(\text{FeMnSi})_{13}$) alloys showed good magnetocaloric response retention after extrusion process was used to design thin-walled heat exchanger structures that had a wall thickness of about 300 microns. Higher magnetic entropy change was achieved ($11\text{J/Kg}\cdot\text{K}$) was retained after the printing process, given that post processing (sintering) was undergone to dilute binder material used for extrusion process. However, the composition does not provide for a structurally stable design and requires large binder volume per gram of magnetocaloric material used for printing. Laser melting processes utilized on LaFeCoSi alloys of different nominal compositions showed lower magnetocaloric performance after additive manufacturing as high energy laser processes could affect magnetocaloric performance due to the repeated melting and recrystallization of magnetic particles. The regenerators fabricated via LBM were seen to be stable in normal atmosphere, as majority of the composition of the material was α -Fe phase and there were efforts made towards decreasing the number of structural strains that happened during the solidification process. However, heat treatment processes undergone to attain desired 1:13 phase left the block structure to disintegrate in the air over a period of 24 hours and then 1 hour after being exposed to distilled water infused with a corrosion inhibition agent. Poor chemical stability was seen and was ultimately attributed to the high temperature ranges undergone during the quenching process that eventually caused internal strains and secondary phase formations. Both processes had effects on the overall stability and performance of the alloys which made extrusion-based processing on this study's specified composition of the LaFeCoSi alloy a suitable choice of processing to produce a solid structure.

The extrusion-based 3D printing method utilized in this experiment provided superior design flexibility in terms of choosing honeycomb structures for heat transfer channels and scaffold-like structures that had porous channels. However, as seen by the magnetic measurements on the 3D printed alloys, magneto functional properties are sacrificed for the process therefore deeming it less attractive. However, solid/powder processing techniques can be utilized to alleviate the issues that arise with 3D printing magnetocaloric structures.

Table 4: Various additive manufacturing methods used for producing magnetocaloric regenerators

| Manufacturing Process | Material System | Part Description |
|-------------------------|--|---|
| Powder Extrusion | $\text{La}_{0.7}\text{Ce}_{0.3}(\text{FeMnSi})_{13}$ | Double-sided comb-like structure (wall thickness of 300 μm ; spacing 700 μm) [43] |
| Selective Laser Melting | $\text{La}(\text{Fe},\text{Co},\text{Si})_{13}$ & steel powder | $\text{La}(\text{Fe},\text{Co},\text{Si})_{13}$ block with wavy-channel geometry (10 x 10 x 30 mm^3 with 500 μm microchannel geometry) and steel powder block with 300 μm microchannel geometry. Transverse fin-shaped rods in a staggered 6 x 21 array were also printed using both powders. [44] |
| Laser Beam Melting | $\text{La}_{0.84}\text{Ce}_{0.16}\text{Fe}_{11.5}\text{Mn}_{1.5}\text{Si}_{1.3}\text{H}_x$ | Nature inspired flow structure and straight flow channels (0.35 mm in diameter) [45] |
| Laser Beam Melting | $\text{La}(\text{Fe}, \text{Si})_{13}$ | Circular geometry with microchannels (spatial resolution of channels; 500 μm) [46] |

Regardless of the lowered magnetocaloric response in the polymer blended solid samples, in-operando stability of magnetocaloric LaFeSiCo alloys show poor chemical stability in both precursor powder and processed solid form. Precursor powder samples show high formation of oxide phases in the material system where the oxidized phases are that of magnetic La-rich phases which highly affects the magnetic properties of the material. 3D printed pieces are structurally not feasible for chemical stability analysis as the soluble polymer binder would be removed from the material system when under immersion. However, it is to be expected that since oxidation affected the magnetic properties of the precursor particles, the magnetic properties of the printed pieces will also be affected negatively indicating poor chemical stability of the LaFeCoSi material alloy.

5.2. Future Work

Active Magnetic Regenerator (AMR) design highly depends on the mechanical and chemical stability of chosen magnetocaloric material. The poor chemical stability of LaFeSiCo alloys presents a challenge to the material's usability as a regenerator in its current state. Additive manufacturing techniques such as the extrusion 3D printing technique used in this study are still primal candidates for designing regenerator geometry for the ability to adjust microchannel dimensions as well as general structure and shape. However, additional processing methods need to be applied to the material to preserve its mechanical and chemical stability after the printing process.

An optimal process to retain 3D printed geometry without the need for polymer binders is solid state sintering of printed solutions. Solid state sintering is a process by which the particles of a material are bonded and densified by the application of heat below the melting point of a material. This process is usually employed for high-quality technical ceramics as the process involves high temperature processing over long periods of time. However, lower temperature treatment can be used to evaporate binder material out of the system which normally has a significantly lower melting point than the magnetocaloric material. High temperature treatments can then be utilized to sinter the particles for fusion. Research to this end is ongoing at Advanced Magnetic Material Processing Laboratory at Virginia Commonwealth University.

6 References

- [1] IEA, "World Total Energy Supply by Source," 2021.
- [2] "Nuclear Power," 21 11 2021. [Online]. Available: <https://www.nuclear-power.com/nuclear-engineering/thermodynamics/thermodynamic-cycles/heating-and-air-conditioning/vapor-compression-cycle-vapor-compression-refrigeration/>. [Accessed 01 05 2022].
- [3] R. Slagle, "How Vapor-Compression Cooling Works," 21 07 2017. [Online]. Available: <https://www.electronics-cooling.com/2017/07/vapor-compression-cooling-works/#:~:text=The%20heart%20of%20the%20system,to%20either%20air%20or%20water..> [Accessed 01 05 2022].
- [4] Office of Energy Efficiency and Renewable Energy, "5 New Air Conditioning Technologies to Keep You Cool," 03 08 2017. [Online]. Available: <https://www.energy.gov/eere/articles/5-new-air-conditioning-technologies-keep-you-cool>. [Accessed 01 05 2022].
- [5] "Thermoacoustics - Professor Artur J. Jaworski," [Online]. Available: <https://sites.google.com/site/professorarturjjaworski/thermoacoustics>.
- [6] T. Chiba and T. Komine, "Thermoelectric refrigerator based on asymmetric surfaces of a magnetic topological insulator," *AIP Advances*, 2020.
- [7] "History of Thermoelectrics," Northwestern University, [Online]. Available: <http://thermoelectrics.matsci.northwestern.edu/thermoelectrics/history.html>. [Accessed 01 05 2022].
- [8] B. Wolf, Y. Tsui, D. Jaiswal-Nagar, U. Tutsch, A. Honecker, K. Remović-Langer, G. Hofmann, A. Prokofiev, W. Assmus, G. Donath and M. Lang, "Magnetocaloric effect and magnetic cooling near a field-induced quantum-critical point," *Proceedings of the National Academy of Sciences*, vol. 108, no. 17, pp. 6862-6866, 2011.
- [9] D. Brown, N. Fernandez, J. Dirks and T. Stout, "The Prospects of Alternatives to Vapor Compression Technology for Space Cooling and Food Refrigeration Applications," US Department of Energy, 2010.
- [10] J. Lyubina, "Magnetocaloric Materials for Energy Efficient Cooling," *Journal of Physics D: Applied Physics*, 2017.
- [11] A. Tishin, "Magnetocaloric effect in the vicinity of phase transitions," *Handbook of Magnetic Materials*, vol. 12, no. 1999, pp. 395-524.
- [12] "Magnetocaloric effect," [Online]. Available: [https://www.sciencedirect.com/topics/chemistry/magnetocaloric-effect#:~:text=Magnetocaloric%20effect%20\(MCE\)%20is%20a,transitions%20concomitant%20with%20magnetic%20transitions..](https://www.sciencedirect.com/topics/chemistry/magnetocaloric-effect#:~:text=Magnetocaloric%20effect%20(MCE)%20is%20a,transitions%20concomitant%20with%20magnetic%20transitions..) [Accessed 01 05 2022].

- [13] X. Moya and N. Mathur, "Caloric Materials for Heating and Cooling," *Science*, vol. 370, no. 6518, pp. 797-803.
- [14] A. Smith, "Who discovered the magnetocaloric effect," *The European Physics Journal H*, vol. 38, pp. 507-517, 2013.
- [15] "Astronautics Corporation of America," ARPA.E, [Online]. Available: <https://arpa-e.energy.gov/technologies/projects/air-conditioning-magnetic-refrigeration>. [Accessed 01 05 2022].
- [16] A. Kitanovski, J. Tusek, U. Tome and u. Plaznik, "Magnetocaloric energy conversion," *Springer International Pu*, 2016.
- [17] V.Franco, J.S.Blázquez, J.J.Ipus, J.Y.Law, L.M.Moreno-Ramírez and A.Conde, "Magnetocaloric Effect: From materials research to refrigeration devices," *Program of Materials Science*, vol. 93, pp. 112-232, 2018.
- [18] S. Wojcieszak, B. Wodajo, A. Duong, R. L. Hadimani and R. Barua, "Review of Studies on Chemical Stability and Corrosivity of Magnetocaloric Materials," *Journal of Materials. Accepted, In Press; ce*, 2021.
- [19] W.H.Wang, Z.G.Zheng, B.Huang, J.W.Lai, Q.Zhou, L.Lei and D.C.Zeng, "Magnetocaloric effect. corrosion and mechanical properties of Mn_{1.05}Fe_{0.9P0.5}Si_{0.5}Cu alloys," *Intermettals*, vol. 113, no. 106539, 2019.
- [20] A. Kitanovski and P. W. Egolf, "Innovative ideas for future research on magnetocaloric technologies," *International Journal of Refrigeration*, vol. 33, no. 3, pp. 449-464, 2010.
- [21] K. Engelbrecht, C. R. H. Bahl and K. K. Nielsen, "Experimental results for a magentic refrigeration using three different types of magnetocaloric material regenerators," *International Journal of Refrigeraiton* , vol. 34, no. 4, pp. 1132-1140, 2011.
- [22] I. A.Radulova, K. P.Skokova, D. Yu.Karpenkovab, T. Gottschalla and O. Gutfleischa, "On the preparation of La (Fe, Mn, SI) 13Hx polymer-composites with optimized magnetocaloric properties," *Journal of Magnetism and Magnetic Materials*, vol. 396, pp. 228-236, 2015.
- [23] T. Lei, K. Engelbrecht, K. K.Nielsena and C. T.Vejeb, "Study of geometries of active magnetic regenerators for room temperature magentocaloric refrigeration," *Applied Thermal Engineering*, vol. 111, pp. 1232-1243, 2017.
- [24] I. Gibson, D. Rosen, B. Stucker and M. Khorasani, *Additive manufacturing technologies*, Cham, 2021.
- [25] K. S. Prakash, T.Nancharaih and V. S. Rao, "Additive manufacturing techniques in manufacturing-an overview," *Materials Today: Proceedings*, vol. 5, no. 2, pp. 3873-3882, 2018.
- [26] M. S. Kamran, J. Sun, Y. B. Tang, Y. G. Chen, J. H. Wu and H. S. Wang, "Numerical investigation of room temperature magnetic refrigerator using microchannel regenerators," *Applied Thermal Engineering*, vol. 102, pp. 1126-1140, 2016.

- [27] C. Hunt, R. Barua and E. Carpenter, "Influence of A-Site cation size-disorder on the magnetocaloric response of $\text{La}_{0.6}\text{Ca}_x\text{Sr}_{0.4-x}\text{MnO}_3$ nanoparticles," *AIP Advances*, vol. 10, 2020.
- [28] M. Balli, S. Jandi, P. Fournier and A. Kedous-Lebouc, "Advanced materials for magnetic cooling: Fundamentals and practical aspects," *Applied Physics Reviews*, vol. 4, no. 2, 2017.
- [29] V. Franco, J. S. Blazquez, B. Ingale and A. Conde, "The magnetocaloric effect and magnetic refrigeration near room temperature: materials and models," *Annual Review of materials Research*, vol. 42, pp. 305-342, 2012.
- [30] T. Hartnett, V. Sharma, S. Garg, R. Barua and P. V. Balachandran, "Accelerated design of MTX alloys with targeted magnetocrystallographic properties through interpretable machine learning," *Acta Materialia*, vol. 231, 2022.
- [31] D. Clifford, V. Sharma, K. Deepak, R. V. Ramanujan and R. Barua, "Multicaloric Effects in $(\text{MnNiSi})_{1-x}(\text{Fe}_2\text{Ge})_x$ Alloys," *IEEE Transactions on Magnetics*, vol. 57, no. 2, 2020.
- [32] K. Javed, S. Gupta, V. K. Pecharsky and R. L. Hadimani, "Stability of Magnetocaloric $\text{La}(\text{Fe}_x\text{Co}_{1-x})_{13}$ in water and air," *AIP Advances*, vol. 9, no. 3, 2019.
- [33] "Scanning Electron Microscopy," Nanoscience Instruments, 01 03 2022. [Online]. Available: <https://www.nanoscience.com/techniques/scanning-electron-microscopy/>. [Accessed 01 05 2022].
- [34] "X-ray powder diffraction," 21 04 2021. [Online]. Available: https://serc.carleton.edu/msu_nanotech/methods/XRD.html. [Accessed 01 05 2022].
- [35] X.-R. d. (. :. A. P. Wiki, Anton Paar. [Online]. [Accessed 01 05 2022].
- [36] S. V. Borisov and N. V. Podberezskaya, "X-ray diffraction analysis: A brief history and achievements of the first century," *Springer Link*, vol. 53, pp. 1-3, 2012.
- [37] I. Rodríguez, R. Gautam and A. D. Tinoco, "Using X-ray Diffraction Techniques for Biomimetic Drug Development, Formulation, and Polymorphic Characterization," *Biomimetics*, 2021.
- [38] R. K. McDonald, "Characterisation Methods of Organic Thin Films with Applications Toward Implantable Bionic Devices," 2007.
- [39] "Physical Property Measurement System," Quantum Design North America - Products - PPMS® DynaCool™ – Quantum Design, [Online]. Available: <https://www.qdusa.com/products/dynacool.html>. [Accessed 01 05 2022].
- [40] "Vibrating-sample magnetometer," Wikipedia, 21 May 2021. [Online]. [Accessed 04 May 2022].
- [41] Y. Su, Y. Sui, J. Cheng, X. Wang, Y. Wang and W. Liu, "Magnetocaloric properties of single crystalline YbTiO_3 with second order phase transition," *Journal of Physics: Conference Series*, vol. 400, 2012.
- [42] J. Israelachvili, "The different faces of poly(ethylene glycol)," *Proceedings of the National Academy of Sciences*, vol. 94, no. 16, pp. 8378-8379, 1997.

- [43] S. Wieland and F. Petzoldt, "Powder-extrusion and sintering of magnetocaloric LaCe (FeMnSi) 13 alloy," *Journal of Alloys and Compounds*, vol. 719, pp. 182-188, 2017.
- [44] J. D. K. D. Moore, D. Lindackers, S. Grasmann, R. Träger, J. Eckert and O. ... Gutfleisch, "Selective laser melting of La (Fe, Co, Si) 13 geometries for magnetic refrigeration," *Journal of Applied Physics*, vol. 114, no. 4, 2013.
- [45] K. Navickaitė, J. Liang, C. Bahl, S. Wieland, T. Buchenau and K. & Engelbrecht, "Experimental characterization of active magnetic regenerators constructed using laser beam melting technique," *Applied Thermal Engineering*, vol. 174, 2020.
- [46] S. Wieland, "Additive manufacturing of functional metallic materials," in *EuroPM2019*, 2019.
- [47] B. D. Cullity and C. D. Graham, *Introduction to magnetic materials*, John Wiley and Sons, 2011.
- [48] X. Zhang, B. T. Lejeune, R. Barua, R. W. McCallum and L. H. Lewis, "Estimating the in-operando stabilities of AlFe₂B₂-Based compounds for magnetic refrigeration," *Journal of Alloys and Compounds*, vol. 823, 2020.
- [49] N. Ma, S. Liu, W. Liu, X. L. D. Wei, L. Wang, L. Li, B. Zhao and Y. Wang, "Research Progress of Titanium-Based High Entropy Alloy: Methods, Properties, and Applications," *Frontiers of Bioengineering and Biotechnology*, vol. 8, 2020.